NASA

Technical Memorandum 85047

REMOTE SENSING BY INFRARED HETERODYNE SPECTROSCOPY

Theodor Kostiuk
Michael J. Mumma

JUNE 1983

National Aeronautics and
Space Administration

Goddard Space Flight Center
Greenbelt, Maryland 20771

REMOTE SENSING BY INFRARED HETERODYNE SPECTROSCOPY

Theodor Kostiuk and Michael J. Mumma

Infrared and Radio Astronomy Branch
Laboratory for Extraterrestrial Physics
NASA/Goddard Space Flight Center
Greenbelt, Maryland 20771

ABSTRACT

The use of infrared heterodyne spectroscopy for the study of planetary atmospheres is discussed. Infrared heterodyne spectroscopy provides a convenient and sensitive method for measuring the true intensity profiles of atmospheric spectral lines. Application of radiative transfer theory to measured lineshapes can then permit the study of molecular abundances, temperatures, total pressures, excitation conditions, and dynamics of the regions of line formation. The theory of formation of atmospheric spectral lines and the retrieval of the information contained in these molecular lines is illustrated. Notable successes of such retrievals from infrared heterodyne measurements on Venus, Mars, Jupiter and the Earth are given. A discussion of new developments in infrared heterodyne technology is also presented.

INTRODUCTION

Remote measurement of molecular spectra is a proven method for the study of planetary atmospheres. Analysis of such spectra using related laboratory data and appropriate theory can yield a wealth of information on the physics, chemistry and dynamics of the atmospheric region studied. Results of such measurements and analyses will then lead to improved atmospheric models, contributing to a better understanding of the specific planetary atmosphere studied and providing insight into atmospheric evolution as a whole.

Many molecules of atmospheric and astronomical interest exhibit rotational-vibrational spectra in the middle infrared. As can be seen from Fig. 1, the thermal emission from the terrestrial planets peaks in this spectral region and substantial radiance is also emitted from Jupiter and Saturn. Several good telluric windows exist in this spectral region, enabling remote measurements with minimum interference from major atmospheric absorbers. A particularly good spectral band for ground based measurements of planets and for spectral studies of the Earth's minor atmospheric constituents is the 1000 cm^{-1} atmospheric window. It falls near the peak of the emitted radiances and corresponds to a spectral region where infrared heterodyne and other infrared technology is suitably advanced.

Resolving powers of infrared spectrometers range from $\lambda/\Delta\lambda \sim 10$ to 10^7. They each provide complementary information on the structure and physics of the source. Low resolution instruments ($\lambda/\Delta\lambda \sim 10$) provide information on thermal continua, higher resolution instruments such as Fourier transform spectrometers (FTS) with $\lambda/\Delta\lambda \sim 100\text{-}10^4$ can measure molecular band spectra and pressure broadened spectral lines. Higher resolution instruments (e.g. Fabry-Perot and higher resolution FTS) with $\lambda/\Delta\lambda = 10^4\text{-}10^5$ can measure pressure broadened and turbulence broadened lines. To measure Doppler broadened lineshapes, however, resolving powers of $\gtrsim 10^6$ are required and the remote measurement technique is infrared heterodyne spectroscopy.

The goal of high resolution spectroscopy is to measure and analyze the individual spectral lineshapes and to retrieve the information contained therein

on the region of their formation. The information contained in individual spectral lines is illustrated in Table 1. Measurements of absolute intensity profiles can yield total pressures and altitude profiles of molecular abundances and temperatures. Widths of Doppler lines yield local kinetic temperatures. Under optically thin conditions, integrated intensities yield vibrational temperatures and a relative comparison of the profiles yields rotational temperatures. These results permit the study of local excitation conditions and determine whether the region is in local-thermodynamic equilibrium or not and whether extreme non-LTE phenomena, such as lasing, are present. Absolute line frequency measurements can determine the relative and absolute velocity of the source region and permit the study of local winds and velocity structure and thus local dynamics. Spatial mapping of the above parameters enables the study of their spatial variability, effects of local insolation and contributes to the overall understanding of the atmosphere. Temporal variability studies determine diurnal effects, effects due to local insolation and permit the study of atmospheric photochemistry. Isotopic studies can yield information on elemental abundances and resultant atmospheric chemistry.

To take full advantage of the information content of spectral lines and to retrieve these atmospheric parameters, the true line shapes of molecules must be measured with suitably high signal-to-noise. Some of the most interesting phenomena in the atmospheres of planets occur in low density, low temperature regions where sub-Doppler spectral resolution as well as high spatial resolution are needed to fully resolve the lineshapes and to spatially map the source. Infrared heterodyne spectroscopy offers the necessary spectral resolution $\lambda/\Delta\lambda \sim 10^7$. It offers the required spatial resolution since, being a coherent technique, the field of view is matched to the diffraction limit of the collecting optics (few arc-seconds with typical ground based telescopes). Heterodyne spectroscopy can provide highly specific and accurate frequency measurements. Line position determination is possible to $\sim 1:10^8$. This facilitates species identification from spectral line positions and permits velocity measurements to several meters per second. The technique is also highly sensitive to detection of narrow, nearly Doppler features which would be frequency diluted by most conventional resolving powers.

The basic concepts of heterodyne detection will now be discussed.

Heterodyne spectrometer design and critical system parameters, as they apply to remote measurement of spectral line profiles, will be described using as an example the Goddard Space Flight Center Infrared Heterodyne Spectrometer (IRHS). The theory of formation of the various spectral lines in planetary atmospheres will be briefly described. Actual heterodyne measurements of the various classes of atmospheric lines on Venus, Mars, Jupiter and the Earth will be used to illustrate the retrieval of many of the atmospheric parameters contained within these lines as outlined above. Finally, a discussion of technology which is currently being developed to improve infrared heterodyne spectrometer performance and which is applicable for space flight use will be presented.

INFRARED HETERODYNE DETECTION: THEORY

Figure 2 illustrates the basic concept of heterodyne detection along with some relevant performance equations. Infrared heterodyne detection is achieved by combining the radiation from a source (frequency ω_s, electric field $= E_s e^{i\omega_s t}$) with the output of a laser local oscillator (ω_{LO}, field $= E_{LO} e^{i\omega_{LO} t}$) on a nonlinear infrared detector (photomixer). Classically the total electric field is

$$E = E_{LO} e^{i\omega_{LO} t} + E_s e^{i\omega_s t} \qquad (1)$$

The nonlinear response of the photomixer is[1]

$$R_{IR} = E^* E = E_{LO} E_{LO} + E_s E_s + 2 |E_{LO} E_s| \cos(\omega_{LO} - \omega_s)t \qquad (2)$$

A cross product term is generated at a difference frequency $\omega_{IR} = |\omega_{LO} - \omega_s|$. This frequency is the intermediate frequency (IF). It contains the spectral information of the infrared source and can be amplified, detected and analyzed with appropriate radio frequency electronics.

The time averaged heterodyne signal is,

$$S_{Het} = P_{LO} P_s$$

where,

P_{LO} = local oscillator power

P_s = source power in bandwidth B

The optimum heterodyne performance is achieved when the noise is dominated by shot noise generated by the local oscillator (shot-noise-limited operation). In this case, the signal-to-noise ratio is

$$S/N = \frac{P_s}{h\nu B} \tag{3}$$

where B = bandwidth of the frequency resolving element (e.g. RF filter).

The signal-to-noise ratio can be enhanced by integration over time, τ, and is limited by the degradation of the system from ideal. The Δ factor[2] represents this degradation and includes a factor of 2 for chopping (for synchronous detection), 2 for polarization (heterodyne detection is inherently a polarization dependent technique), the effect of the photomixer heterodyne quantum efficiency and the optical losses in the spectrometer. These and other causes of degradation are discussed in detail elsewhere.[3,4,5] The resultant signal-to-noise ratio is:

$$S/N = \frac{P_s}{\Delta h\nu}\left(\frac{\tau}{B}\right)^{1/2} \tag{4}$$

The noise-equivalent-flux (photons/sec-Hz) is then given by

$$NEF = \frac{\Delta}{\sqrt{B\tau}}\ \frac{\text{photons}}{\text{sec Hz}} \tag{5}$$

and is the measure of the sensitivity of an infrared heterodyne spectrometer.

The above relations neglect the limits to the ideal sensitivity imposed by

low local oscillator power and noise generated by the source and background radiation. A more general treatment of these limits can be found in literature.[3,5]

INSTRUMENTATION

An actual design of an operating infrared heterodyne spectrometer is given in Fig. 3 and Fig. 4. Figure 3 illustrates the optical front end of the Goddard Space Flight Center Infrared Heterodyne Spectrometer.[4,6] A signal from a remote source, ν_{IR}, as seen through the telescope is chopped against a reference beam, which can be either a portion of nearby sky or a calibrated blackbody reference. In the sky chopping mode the bow-tie mirror chopper switches the beam $\lesssim$ 30 arc seconds off the source every other half cycle at a chopping frequency of $\sim$23 Hz. In the balanced radiometer mode the source is chopped against a matched blackbody. For intense sources (e.g. the Sun) a solar filter is used to limit the bandwidth of the incident radiation and thus to minimize synchronously detected source shot noise. The chopped beam is focused in the primary focal plane and then collimated by an off-axis parabolic mirror. The output from a grating tuned, line center stabilized CO_2 laser (ν_{LO}) is attenuated, expanded and collimated to match the signal beam. The two beams are combined at the ZnSe beamsplitter and then focused onto a HgCdTe photomixer[7] with a second off-axis parabolic mirror. The IF difference frequencies are then amplified and fed into the 128 channel spectral line receiver (Fig. 4) where integration and synchronous detection takes place.[6,8]

The input IF power is split between two filter banks--the low resolution bank consisting of 64 contiguous 25 MHz RF filters covering a fixed bandwidth of 0 to 1.6 GHz (0.053 cm^{-1}) (resolving power $\lambda/\Delta\lambda \sim 10^6$) and a tuneable high resolution bank consisting of 64, 5 MHz RF filters. The 320 MHz bandwidth in the IF covered by the high resolution filter bank can be tuned to any portion of the low resolution filter bank by mixing the IF input with the output of a tuneable RF local oscillator. This permits the measurement of spectral features within the low resolution bank at 5 times the resolving power. The chopper reference signal is used for a clock. At the end of each half of the chopping cycle the output of filters is detected, multiplexed, digitized and stored in a buffer memory. The signal (S) and reference (R) portions of the chopping cycle

are stored separately. After a preselected integration time the data are dumped into an LSI-11 mini-computer where synchronous detection is done analytically yielding the resultant signal, (S-R)/(R-Z). The zero-input voltages (Z) of the filter bank channels are measured separately with the RF input fully attenuated. The data are automatically stored on a dual floppy disc. Some on-line analysis can be done and the raw or manipulated data can be displayed on a CRT terminal. Hard copies can be made using a copier, x-y plotter or line printer.

An example of the data output, as displayed on the terminal screen, is shown in Fig. 5c. The spectral feature at 1300 MHz IF frequency in the low resolution filter bank (left side) is shown centered in the 5 MHz high resolution bank (on the right).

PERFORMANCE PARAMETERS

The GSFC IRHS will now be used to illustrate the important performance parameters of such systems and their practical limits as they apply to remote spectral studies. Spectral resolution, tuneability, spatial resolution and sensitivity will be discussed.

Spectral Resolution

To illustrate spectral resolution let us look at measurements of the same source (Venus) using three classes of instruments (Fig. 5). Figure 5a shows the results of photometric measurements with resolving powers $\lambda/\Delta\lambda \sim 1$. A broadband radiance plot is obtained. If a small spectral region near 1000 cm^{-1} is studied at higher resolution, a complex molecular absorption structure (Fig. 5b) is revealed.[9] Results at $\sim$0.25 cm^{-1} resolution obtained by Fourier transform spectroscopy, are compared with modelled spectra in Fig. 5b. The resolution is sufficient to resolve the individual CO_2 absorption lines in the 10μm lasing band, but not sufficient to resolve the individual line profiles where much of the information about the region of their formation is contained.

A measurement of a single R8 transition near 967.707 cm^{-1} with the Goddard heterodyne spectrometer reveals a narrow emission line (Fig. 5c). This emission is Doppler shifted from the CO_2 rest frequency by $\sim$1300 MHz (low resolution

bank) due to the geocentric velocity of Venus at the time of observation. The high resolution bank adequately measures the line profile of the nonthermal core emission line (50 MHz wide, 320K brightness temperature). The R8 absorption line exceeds the width of the filter bank, and the emission feature is centered near the expected position of the absorption minimum. Note that the off line continuum is only ~230K (Fig. 5b).

These non-thermal lines of the 10.6μm band of CO_2 were discovered by Betz et al.[10] using an infrared heterodyne spectrometer, and were used by them to derive wind velocities in the high altitude regions (120 km) where the lines are formed. Deming et al.[11] analyzed Goddard IRHS measurements of the CO_2 absorption features. Results yielded evidence of a high altitude haze thickening on the dark side of Venus between 15 and 35 mbar pressures.[11]

Tuneability

The gross spectral tuneability of infrared heterodyne spectrometers is determined mainly by tuneability of the laser local oscillator. Although tuneable diode lasers have been used as local oscillators in heterodyne receivers,[12-16] highly sensitive heterodyne spectrometers require the power, noise and mode structure available from gas lasers (CO_2, N_2O). Molecules emit in discrete line frequencies. With low pressure gas lasers $\lesssim$20 MHz tuning can be achieved over a single line. This limits the spectral coverage to small bands (photomixer bandwidth) about each laser transition. Some additional tuneability can be obtained by use of higher pressure waveguide lasers (cf. Ref. 21). In this case, however, as with diode lasers, absolute local oscillator frequencies are less accurately known.

The most commonly used laser local oscillator, the CO_2 laser has transitions from 9-12μm if all the isotopes of CO_2 are used. (See Fig. 6 taken from Freed et al.[17]). Even with lines from all these isotopes of CO_2 and a photomixer bandwidth of ~2 GHz only ~15% of this spectral region will be covered. Fortunately many molecules of atmospheric and astronomical interest have molecular bands within this region and many near coincidences between their spectral lines and CO_2 and N_2O lasing transitions exist. Because of the narrow bandwidth and lack of tuneability, high accuracy, sub-doppler laboratory

measurements are required to determine the molecular line positions and to identify those lines which fall within the necessary frequency offset from the CO_2 laser transitions.[18-20]

Table 2 lists molecules with ro-vibrational bands in the 9-12μm region and those which have been measured remotely using gas laser infrared heterodyne techniques.[21-29]

Sensitivity

The sensitivity of a spectrometer can be measured by the minimum blackbody radiation it can detect. This indeed is a good parameter since in an optically thick region molecules in local thermodynamic equilibrium cannot radiate above the Planck function for the local temperature, while absorption lines are measured against a continuum blackbody-like source such as the Sun or planetary surface. The spectral radiance, including both polarizations, of a blackbody is given by

$$N = \frac{2}{\lambda^2 (e^{h\nu/kT} - 1)} \quad \frac{\text{photons}}{\text{sec Hz cm}^2 \text{ sr}} \tag{6}$$

The etendue of heterodyne receivers is given by the antenna theorem[30]

$$A\,\Omega_A \sim \lambda^2 \quad \text{cm}^2 \text{ sr} \tag{7}$$

Where λ is the wavelength, A is the effective aperture and Ω is the beam solid angle defined as in usual antenna theory. The throughput is thus independent of the collecting optics. The heterodyne field of view can thus be matched to the diffraction limit of the collecting optics (e.g. for a 55 inch telescope the field of view (FWHM) corresponds to ~1.8 arcsec at λ = 10μm). This permits mapping of small sources (e.g. Mars) from the ground, and allows high altitude resolution in limb scanning measurements from balloons or from planetary orbit.

Combining Eqs. (6) and (7), the single sideband[6] spectral intensity (F) collected in a heterodyne field of view is

$$F = \frac{2}{e^{h\nu/kT} - 1} \quad \frac{\text{photons}}{\text{sec Hz}} \qquad (8)$$

Neglecting noise generated by source radiation and gain non-linearities in the electronics and using Eq. 5 the post-integration signal-to-noise ratio is

$$S/N = \frac{2\sqrt{B\tau}}{\Delta(e^{h\nu/kT} - 1)} \qquad (9)$$

Operating infrared heterodyne spectrometers exhibit an increase in the Δ factor (and thus a decrease in signal-to-noise ratio) as a function of IF frequency due to the roll-off of the response of the photomixer and preamplifier. In the Goddard infrared heterodyne spectrometer, the measured Δ increases from $\Delta \sim 7$ at frequencies near the local oscillator (<400 MHz) to ~ 20 at 1.6 GHz.

The spectral intensity is plotted in Fig. 7 as a function of wavelength for various blackbody temperatures. The NEF for an optimized field system with $\Delta = 7$, B=25 MHz and an integration time of 1 hour is given by the dashed line. The range of temperatures observed on various sources is indicated by the bracketed lines. The corresponding signal-to-noise ratio for a given source spectral intensity can be directly determined and is shown on the right vertical axis. For example, at 10.3μm, measurement of Mars' equatorial continuum ($\sim$250 K) would yield a S/N $\sim$400. Measurements at 12μm on Jupiter ($\sim$150 K) would yield a S/N $\sim$40. In the 9-12μm region thermal radiation from most planets is observable with this heterodyne sensitivity. The infrared spectral intensity of the Sun ($\sim$5100 K) is $\sim$7 at 10μm. For the given instrumental sensitivity this yields a formal S/N $>$ 300,000 on the continuum and 300 on absorption lines 0.1 % deep. However, source noise and instrumental effects can substantially reduce the signal-to-noise ratio on hot sources.[5]

FORMATION OF ATMOSPHERIC SPECTRAL LINES

Figure 8 illustrates the formation of spectral lines in a planetary atmosphere. The total intensity incident on an observer looking through an intervening atmosphere of total transmittance τ_s, at a thermal source, $I_s(\nu,T_s)$, such as a planetary surface or the Sun, is composed of transmitted intensity from the source, $I_s(\nu,T_s)\ \tau_s(\nu)$ and the self-emission of the intervening atmosphere. Each atmospheric layer has an emissivity $\varepsilon_L(\nu)$ and transmittance $\tau_L(\nu)$. This total upwelling radiance from an atmosphere can be written.[31,32]

$$I_{TOTAL}(\nu) = I_s(\nu,T_s)\ \tau_s(\nu) + \int_{\tau_s}^{1} B(\nu,T(P))\ d\tau \qquad (10)$$

where

$I_s(\nu,T_s)$ = $\varepsilon_s(\nu)B_s(\nu,T_s)$
$B(\nu,T)$ = the Planck function at temperature T
$\varepsilon_s(\nu)$ = surface emissivity
τ = $\exp\left(-\int_z^{\infty} K_\nu n(z)dz\right)$
$n(z)$ = the number density at height z
K_ν = the absorption coefficient at frequency ν
$P(z)$ = pressure at altitude z

An external observer can probe into the atmosphere to about one optical depth, where the thermal radiance at a frequency ν will be a function of the temperature T at that depth and, in LTE, will be Planckian. Since the absorption coefficient varies with frequency (spectral lines), different regions of the atmosphere can be probed by measuring line profiles, probing deeper into the atmosphere in regions of weak absorption (line wings) and less so in regions of strong absorption (line center).

An inverse or iterative solution of Eq. 10 using such line profile measurements permits the retrieval of atmospheric density or pressure as a function of altitude if the temperature profile is known.[25,33] Conversely if the density profile is known, the temperature profile can be determined.[32,33] The quality of the inverted profile is limited by the signal-to-noise ratio on the $I_{TOTAL}(\nu)$ (measured line), the accuracy of molecular line or band parameters used (strength, frequency, pressure broadening, Doppler width) and the

temperature dependence of K_ν.

In most cases high signal-to-noise ratios can be obtained using infrared heterodyne techniques. Heterodyne spectroscopy permits the measurement of individual line profiles at sub-Doppler resolution, therefore, minimizing competitive effects which enter in when blended lines are measured at lower spectral resolution. For determining temperature as a function of altitude, a line whose lower state population is strongly dependent on the local temperature can be measured for maximum temperature resolution. If a density profile is desired, a line whose lower state population is nearly independent of temperature can be chosen. This kind of tailoring of the measurements is not possible at lower resolution when entire molecular bands must be used.

OBSERVATIONS AND RETRIEVAL

As was discussed above there are three classes of lines formed in planetary atmospheres, depending on local physical conditions and on the molecular physics of the line forming species - lines that consist of pure absorption of a source continuum, (first term on the right hand side of Eq. 10) lines that consist mainly of molecular self emission (the second term on the right hand side of Eq. 10), including non-thermal emission, and lines which are made up of both contributions. Examples of these three classes of atmospheric lines will now be given and the retrieval of many of the relevant atmospheric parameters shown in Table 1 from infrared heterodyne measurements will be illustrated.

The CO_2 lines in the $00^0 1 - [10^0 0, 02^0 0]_{I,II}$ bands on Mars are an example of composite atmospheric lines. Figure 9A shows the major contributions to the measured line profile. The observed R(8) feature, measured at 10.33μm with 25 MHz resolution (circles), is composed of the transmitted Mars surface intensity, the atmospheric self emission (light shading) and a high altitude non-thermal emission plus laser contribution (dark shading).[23,34]

In the absence of significant continuum absorption (local dust storms or clouds) the emergent intensity far from line center is a measure of surface temperature. Calibrating our instrument against a known temperature source (e.g. the Moon), Mars surface temperatures were derived.[23,35] Using Mars

temperature profiles from Viking results,[36] the broad wing absorption line was modelled and fit to the measured data (iterative solution of Eq. 10). This analysis permitted the retrieval of surface pressures at various locations on the planet.[35] The derived temperatures and pressures agreed well with values derived from Viking lander and Mariner 9 orbiter data.[37]

Analysis of the core emission peak (Fig. 9B) permitted the retrieval of the local kinetic temperature (~110-150K) from the line halfwidth and the vibrational temperature from the integrated intensity. Using these results it was shown that a population inversion of the CO_2 ν_3 and $2\nu_2$ levels was present at altitudes above 60 km on Mars and optical gain was demonstrated; the necessary and sufficient conditions for a natural CO_2 laser.[23] This Mars CO_2 laser is pumped by solar radiation in the near infrared bands and detailed theoretical modelling of these bands on Mars confirm the observational results.[38] Results are consistent with additional analysis of observations on several rotation lines (J=4 to J=20) and comparison of relative intensities of these CO_2 lasing transitions on Mars yielded a rotational temperature of 135 ± 20K.[34]

Figure 10 illustrates a partial global map of the CO_2 R8 line on Mars. The heterodyne beam field-of-view on the planet was ~1.8 arc-seconds (FWHM). The observing geometry on a 13 arc-second planetary disc is shown in the upper right. Some qualitative conclusions are evident from these observations. At the time of observation the subsolar point on the planet was located in the northeastern quadrant of the disc, therefore, the solar pumped laser emission is observed to be most intense in the north, east, and center measurements. The surface temperature, however, (as measured by the intensity far from line center) is cool in the morning (east limb), hot near noon and afternoon (center and west limb) and is hotter in the north than the south (northern summer).

Let us now examine infrared heterodyne measurement of ethane emission lines from the stratosphere of Jupiter[29] as examples of nearly pure self emission lines. The geometry of observation is shown in Fig. 11 where the ~2 arc sec beam is positioned at the south polar region of the 40 arc-sec planetary disc. The observational results are presented in Fig. 12, where the intensities of the individual 25 MHz-wide channels (circles) are plotted as brightness temperature

vs. frequency relative to the center of the stronger J=17 peak (dashed curve). The dashed curve is a calculated spectrum (Eq. 10) as it would appear in the absence of instrumental or Jovian rotational broadening. The direct solution of the radiative transfer equation used an appropriate atmospheric model, including a Voyager 2 temperature profile for 70^{o} south latitude. The solid curve represents the spectrum convolved with an appropriate rotational broadening function. The line-of-sight component of Jovian rotational velocity varies across our field-of-view and, thus, introduces a velocity broadening corresponding to ~200 MHz. It is the solid curve which is fit to our data. The retrieved parameter is a constant $C_2H_6:H_2$ volume mixing ratio of 1.2×10^{-6}. This result is consistent with recent photochemical models.[29]

The Jovian atmospheric model used in the analysis is presented in Fig. 13, where the temperature profile obtained from Voyager 2 data is shown. The Voyager infrared spectrometer (IRIS) measured the ethane band in emission near 12μm.[39] Because of the low spectral resolving power ($\lambda/\Delta\lambda$ ~200), information could be retrieved directly only from altitudes corresponding to pressures greater than ~30 mbar (T=135K, see Fig. 13). It is evident from the observed brightness temperatures (Fig. 12) and from the weighting functions (Fig. 13) that the heterodyne measurements can probe from 100 mbar to ~1 mbar pressure levels (160-170K).[29]

The remaining example is an infrared heterodyne measurement of spectral lines where the source intensity is so bright that the self emission contribution from the intervening atmosphere is negligible. Such a situation is obtained in atmospheric absorption measurements against the Sun. As was discussed earlier this geometry permits high signal-to-noise measurements on weak atmospheric lines. Actual measurements of signal-to-noise of ~40 on 0.1% deep atmospheric lines have been achieved at 25 MHz resolution and 1 hour integration time by balancing the Sun against a 1300K blackbody in our heterodyne spectrometer. This "null balanced radiometer" mode of operation eliminates significant noise contributions due to gain non-linearities in the RF system when the signal and reference beams are at greatly different levels. In this way the measurement and study of minor constituents of the Earth's atmosphere is possible. A constituent of particular interest is ClO, which is believed to play a major role in the destruction of ozone in the Earth's

stratosphere.[40]

Because of the inherent narrow bandwidth and limited tuneability of the infrared heterodyne spectrometer, very accurate knowledge of line frequencies of the target molecule is needed so that the lines in near coincidence with the CO_2 local oscillator transitions can be chosen. In addition, it must be determined that the spectral regions observed are clear of spectra of major atmospheric absorbers (e.g. water) that will interfere with the measurements and calibration. In our attempt to measure atmospheric C&O we used accurate line positions obtained by Maki et al.[41] and the atlas of atmospheric transmission of Goldman et al.[42] (Fig. 14). There are three suitable transitions of the $^{35}C\&^{16}O$ molecule which nearly overlap with transitions of the $^{14}C^{16}O_2$ laser local oscillator the C&O R(9.5) line near $^{14}CO_2$ P(12), the R(12.5) line near P(8) and the R(6.5) near P(16). Balloon borne infrared heterodyne measurements were made using the P16 $^{14}CO_2$ transition by Menzies et al.[21] Ground based measurements of the spectral regions near the P8 and P12 laser transitions were made by our group.[22]

Fig. 14 shows the position of the three laser lines in the solar absorption spectrum. Note that even at large air mass the transmittance in the region near P12 is nearly 1 and only weak nitric acid spectra are observed near the laser line position. On the wavenumber scale shown, the bandwidth of the heterodyne spectrometer is only slightly wider than the thickness of the drawn lines. Infrared heterodyne measurements of pure absorption lines near the spectral region about the P12 laser transition are presented in Fig. 15. Using a standard atmospheric temperature and total pressure profiles as a function of altitude,[43] the observed spectra were modelled. The measured low and high resolution data are compared to spectra modelled using Eq. 10 and published and measured molecular parameters[44-46] and accepted altitude profiles[47-52] of interfering molecules HNO_3, NO_2 and OCS. The C&O lines were modelled based on the average altitude profiles obtained by Anderson[53] and available line strengths[54] and pressure broadening coefficient.[55] Agreement between the measured and modelled spectra appear very good. However, no significant structure was seen in the measurements at the position of the modelled C&O lines. The lack of C&O is most graphic in the high resolution spectrum (plotted on the right) where the 0.2% nitric acid line is clearly visible near 550 MHz.

Based on the minimum line depth observable with the obtained signal-to-noise, an upper limit on atmospheric $C\ell O$ abundance can be set. The resultant $C\ell O$ column density is a factor of 7 less than the accepted value of 1.6×10^{14} cm^{-2} at the 95% confidence level (see Ref. 22 for details). Heterodyne measurements by Menzies[21] also show disagreement with the accepted values.

FUTURE DIRECTIONS

Although, through these examples, ultra high resolution infrared heterodyne spectroscopy has been shown to be an extremely powerful technique for measurement of individual spectral lines and the retrieval of salient atmospheric parameters, the method is still limited by the lack of tuneability and spectral coverage in the optical front end, and for space flight application by the size, weight, and power requirements of the associated RF electronics. Future technological advances will be concentrated in these areas. Microwave-laser mixing in wideband electro-optic modulators (e.g. GaAs) can generate tuneable optical sidebands of the CO_2 laser local oscillator and thus extend the coverage of the 9-12μm spectral region to ~50%.[56] Semiconductor diode lasers offer the possibility of semi-continuous tuning over ~100 cm^{-1} in spectral regions from 3-30μm. Diode lasers were first used as local oscillators by Mumma et al.[12] and later by Frerking and Muelhner[15] and by Harward and Hoell[16]. Although these instruments offered the potential of wider continuous tuneability, their sensitivity was quite low due to the low power output and high noise characteristics of available diode lasers. We have recently developed a diode laser heterodyne spectrometer capable of operation from 8-13μm, which is only 5 to 10 times less sensitive than the CO_2 laser system[13] and we have used it for atmospheric and solar observations[14]. Although it was useful for observing hot sources such as the Sun the low power and excess noise of the local oscillator also limited its sensitivity and the useful spectral coverage. Improvement in semiconductor diode laser power output, mode structure and noise characteristics must be pursued.

Extending the wavelength coverage of infrared heterodyne receivers to longer wavelength is also important. Not only does it permit the study of many additional species, it also improves the inherent sensitivity of heterodyne spectrometers and, due to the decrease in energy per photon, decreases the

local oscillator power needed to achieve shot-noise-limited operation. The increase in sensitivity at longer wavelengths can be illustrated by referring to Fig. 7. At 10μm the NEF of the optimized heterodyne spectrometer corresponds to detection of a ~130K source with a signal-to-noise S/N=1. A system with similar parameters at 30μm could detect sources well below 50K and could detect the 130K source with S/N > 1000. We are presently supporting the extension of the operating wavelengths of photomixers[57] and diode lasers[58] to 30μm and developing these components for use in long wavelength heterodyne spectrometers.

The final improvements lie in miniaturization of the optical front end and the development of compact acousto-optic spectrometers (AOS) to replace the large, heavy and power consumptive RF filter bank. CO_2 waveguide lasers have been proposed for space systems[59] and the development of RF excited waveguide laser local oscillators is being pursued at GSFC. Bulk AOS systems have been built and tested.[60] Some have been used for observations with millimeter wave heterodyne systems.[61] This technique utilizes the acousto-optic Bragg effect in a non-linear medium (e.g. $LiNbO_3$ crystal) to disperse a visible laser onto a linear detector array. The index of refraction in the crystal varies as a function of the IF frequency introduced into the material. Each detector corresponds to the focus of a differently refracted beam and thus a different IF frequency. The frequency resolution can be less than 1 MHz and as many as 1000 channels are possible. This method of IF analysis greatly reduces the size, weight and power requirements and can be further miniaturized by the development of integrated versions.[62]

ACKNOWLEDGEMENT

The authors would like to thank all members of the Infrared Heterodyne Spectroscopy group at Goddard for their contributions to the work described in this paper.

References

1. M. C. Teich, Infrared Detectors, Semiconductors and Semimetals Vol. 5, 361, ed. R. K. Willardson and A. C. Beer, Academic Press (1971).

2. T. Kostiuk, M. J. Mumma, M. M. Abbas and D. Buhl, Infrared Physics 16, 61 (1976).

3. M. M. Abbas, M. J. Mumma, T. Kostiuk and D. Buhl, Appl. Opt. 15, 427 (1976).

4. T. Kostiuk, M. J. Mumma, and D. Zipoy, Proceedings of Heterodyne Systems and Technology Conference, Williamsburg, VA. NASA Conference publication, CP-2138, Pt. 2, 365 (1980).

5. cf. R. H. Kingston, Detection of Optical and Infrared Radiation, Springer-Verlag, New York (1978); R. T. Menzies in Laser Monitoring of the Atmosphere ed. E. D. Hinkley, Chapt. 7, 297, Springer-Verlag, New York (1976). T. G. Blaney, Space Science Reviews 17, 691 (1975); H. Van de Stadt, Th. De Graauw, J. C. Shelton, and C. Veth in Space Optics, eds. B. J. Thompson and R. R. Shannon, 443, National Academy of Sciences, Washington, DC (1974).

6. M. J. Mumma, T. Kostiuk, D. Buhl, G. Chin and D. Zipoy Opt. Eng. 21, 313 (1982). A somewhat earlier version of the present system is described in: M. J. Mumma, T. Kostiuk, and D. Buhl, Opt. Eng. 17, 50 (1978). A discussion of single and double sideband detection is also presented in these references.

7. HgCdTe photomixers were provided by D. L. Spears M.I.T. Lincoln Laboratory and are described in D. L. Spears, Infrared Physics 17, 5 (1977); also D. L. Spears, Physics and Technology of Coherent Infrared Radar, SPIE 300, 174 (1981).

8. D. Buhl and M. J. Mumma, Proceedings of Heterodyne Systems and Technology Conference, Williamsburg, VA. NASA Conference publication CP-2138, Pt. 2,

373 (1980).

9. V. G. Kunde, R. A. Hanel and L. W. Herath, Icarus 32, 219 (1977).

10. A. L. Betz, M. A. Johnson, R. A. McLaren and E. C. Sutton, Astrophysics J. 208, L141 (1976).

11. D. Deming, F. Espenak, D. Jennings, T. Kostiuk and M. J. Mumma, Icarus 49, 35 (1982).

12. M. Mumma, T. Kostiuk, S. Cohen, D. Buhl, and P. C. Von Thuna, Nature 253, 514 (1975).

13. D. Glenar, T. Kostiuk, D. E. Jennings, D. Buhl and M. J. Mumma, Appl. Opt. 21, 253 (1982).

14. D. Glenar, D. Deming, D. E. Jennings, T. Kostiuk and M. J. Mumma. To be published Astrophys J. June (1983).

15. M. A. Frerking and D. J. Muehlner, Appl. Opt. 16, 526 (1977).

16. C. N. Harward and J. M. Hoell, Proceedings of Heterodyne Systems and Technology Conference, Williamsburg, VA, NASA Conference publication CP-2138, Pt. 1, 209 (1980).

17. C. Freed, L. C. Bradley and R. G. O'Donnell IEEE J. Quant. Electr., QE-16, 1195 (1980).

18. T. Kostiuk, M. J. Mumma, J. J. Hillman, D. Buhl, L. W. Brown, J. Faris and D. L. Spears, Infrared Physics 17, 431 (1977).

19. T. Kostiuk, J. J. Hillman and J. L. Faris, J. Mol. Spectrosc. 89, 397 (1981).

20. J. J. Hillman, T. Kostiuk, D. Buhl, J. Novaco, and M. Mumma, Opt. Lett. 1, 81 (1977).

21. R. T. Menzies, Jet Propulsion Laboratory, preprint (1982). The measurements and instrumentation are described in : (a) R. T. Menzies, Geophys. Res. Letters 6, 151 (1979). (b) R. T. Menzies, W. Rutledge, R. A. Zanteson, and D. L. Spears, Appl. Opt. 20, 536 (1981). Results reported in (a) and (b) were incorrect and are re-evaluated in the latest work.

22. M. J. Mumma, J. D. Rogers, T. Kostiuk, D. Deming, J. J. Hillman, and D. Zipoy, to be published, Science, (1983).

23. M. J. Mumma, D. Buhl, G. Chin, D. Deming, F. Espenak, T. Kostiuk, D. Zipoy, Science 212, 45 (1981).

24. M. A. Johnson, A. L. Betz, R. A. McLaren, E. C. Sutton and C. H. Townes, Astrophys. J. 208, L145 (1976).

25. M. M. Abbas, T. Kostiuk, M. J. Mumma, D. Buhl, V. G. Kunde and L. Brown, Geophys. Res. Lett. 5, 317 (1978).

26. J. Hoell, D. Harward and B. Williams, Geophys. Res. Lett. 7 (1980).

27. A. L. Betz, R. A. MacLaren and D. L. Spears, Astrophys. J. (Letters) 229, L97 (1979).

28. A. L. Betz, Astrophys. J. (Letters) 244, L103 (1981).

29. T. Kostiuk, M. J. Mumma, F. Espenak, D. Deming, D. E. Jennings, W. Maguire and D. Zipoy, Astrophys. J. 265, 564 (1983).

30. A. E. Siegman, Proc. IEEE 54, 1350 (1966).

31. cf. R. M. Goody, Atmospheric Radiation, Oxford Clarendon Press (1964); also R. M. Goody and J. C. G. Walker, Atmospheres, Prentice-Hall, Inc. (1972).

32. J. T. Houghton, F. W. Taylor, Rep. Prog. Phys. 36, 827 (1973).

33. M. M. Abbas, V. G. Kunde, M. J. Mumma, T. Kostiuk, D. Buhl and M. A.

Frerking, J. Geophys. Res. 84, 2681 (1979).

34. D. Deming, F. Espenak, D. Jennings, T. Kostiuk, M. J. Mumma and D. Zipoy, Icarus, submitted (1983).

35. T. Kostiuk, F. Espenak, D. Buhl, G. Chin, D. Deming, M. J. Mumma, D. Glenar and D. Zipoy, Bull. Amer. Astron. Soc. 12, 703 (1980).

36. A. Seiff and D. B. Kirk J. Geophys. Res. 82, 4364 (1977).

37. S. L. Hess, J. A. Ryan, J. E. Tillman, R. M. Henry, and C. B. Leovy, Geophys. Res. Lett. 7, 197.

38. D. Deming and M. J. Mumma, Icarus, submitted (1983).

39. R. Hanel, B. Conrath, M. Flasar, V. Kunde, P. Lowman, W. Maguire, J. Pearl, J. Pirraglia, R. Samuelson, D. Gautier, P. Gierasch, S. Kumar, and C. Ponnamperuma, Science, 204, 972 (1979). Also R. Hanel, B. Conrath, M. Flasar, L. Herath, V. Kunde, P. Lowman, W. Maguire, J. Pearl, J. Pirraglia, R. Samuelson, D. Gautier, P. Gierascn, L. Horn, S. Kumar, and C. Ponnamperuma, Science, 206, 952 (1979).

40. cf. F. S. Rowland and M. J. Molina, Rev. Geophys. Space Phys. 13, 1 (1975). For a recent review, see: Causes and Effects of Stratospheric Ozone Reduction: An Update, National Research Council: National Academy Press, Washington, DC (1982).

41. A. G. Maki, F. J. Lovas, and W. B. Olson, J. Mol. Spectrosc. 92, 410 (1982).

42. A. Goldman, R. D. Blatherwick, F. H. Murcray, J. W. Van Allen, C. M. Bradford, G. R. Cook, and D. G. Murcray, "New Atlas of IR Solar Spectra," University of Denver (1980).

43. U.S. Standard Atmosphere, 1976, NOAA-S/T 76-1562, U.S. Government Printing Office, Washington, DC (1976).

44. H. A. Weaver, M. J. Mumma, J. L. Faris, T. Kostiuk, and J. J. Hillman, Appl. Optics, submitted, (1983).

45. J. M. Flaud, C. Camy-Peyret, V. M. Devi, P. P. Das, and K. N. Rao, J. Mol. Spectrosc. 84, 234 (1980).

46. J. S. Wells, F. R. Petersen, A. G. Maki, and D. J. Sukle, Appl. Opt. 20, 1676 (1981).

47. D. B. Barker, J. N. Brooks, A. Goldman, J. J. Kosters, D. G. Murcray, F. H. Murcray, J. Van Allen, and W. J. Williams, IEEE Annals No. 75 CH1004-I, I6-6 (1976).

48. The Stratosphere: Present and Future, Ed. by R. D. Hudson and E. I. Reed, NASA RP 1049, National Aeronautics and Space Administration, Washington, DC (1979).

49. W. G. Mankin, M. T. Coffey, D. W. T. Griffith, and S. R. Drayson, Geophys. Res. Letters 6, 853 (1979).

50. E. C. Y. Inn, J. F. Vedder, B. J. Tyson, and D. O'Hara, Geophys. Res. Letters 6, 191 (1979).

51. R. P. Turco, R. C. Whitten, O. B. Toon, J. P. Pollack, and P. Hamill, Nature 283, 283 (1980).

52. N. D. Sze and M. K. W. Ko, Nature 280, 308 (1979).

53. J. G. Anderson, H. J. Grassel, R. E. Shetter, and J. J. Margitan, J. Geophys. Res. 85, 2869 (1980). See also E. M. Weinstock, M. J. Phillips, and J. G. Anderson, J. Geophys. Res. 86, 7273 (1981).

54. J. R. Gillis and A. Goldman, J. Quant. Spectrosc. Radiat. Transfer 26, 23 (1981). See also R. S. Rogowski, C. H. Barr, W. R. Wade, J. M. Hoell, and G. E. Copeland, Appl. Opt. 17. 1301 (1978).

55. H. M. Pickett, D. E. Brinza and E. A. Cohen, J. Geophys. Res. 86, 7279 (1981).

56. G. W. Sachse, Proceedings of Heterodyne Systems and Technology Conference, Williamsburg, VA, NASA Conference Publication CP-2138, Pt. 2, 399 (1980).

57. D. L. Spears, Proceedings of Heterodyne Systems and Technology Conference, Williamsburg, VA, NASA Conference Publication CP-2138, Pt. 2, 309 (1980).

58. K. J. Linden, J. Electron. Mat. 11, 575 (1982).

59. J. H. McElroy, N. McAvoy, E. H. Johnson, J. J. Degnan, F. E. Goodwin, D. M. Henderson, T. A. Nussmeier, L. S. Stokes, B. J. Peyton and T. Flattau, IEEE 65, 221 (1977).

60. G. Chin, D. Buhl and J. M. Florez, Proceedings of the International Optical Computing Conference, SPIE 231, 30 (1980).

61. T. W. Cole, R. T. Stewart and D. K. Milne, Astron. and Astrophys. 67, 277 (1978).

62. M. C. Hamilton, D. A. Wille, and W. J. Miceli, Opt. Eng. 16, 475 (1977).

TABLE 1.

INFORMATION CONTENT OF SPECTRAL LINES

MEASUREMENT	RETRIEVABLE PARAMETERS
INTENSITY PROFILES	MOLECULAR ABUNDANCES TOTAL PRESSURES KINETIC TEMPERATURE ROTATIONAL TEMPERATURES VIBRATIONAL TEMPERATURES EXCITATION CONDITIONS (LTE, NON-LTE, LASERS)
LINE FREQUENCIES	VELOCITY SHIFTS WINDS
SPATIAL MAPPING	SPATIAL VARIABILITY OF ABOVE PARAMETERS
TEMPORAL VARIABILITY	DIURNAL EFFECTS PHOTOCHEMISTRY
ISOTOPIC STUDIES	ELEMENTAL ABUNDANCES ATMOSPHERIC CHEMISTRY

TABLE 2.

MOLECULES DETECTABLE WITH GAS LASER HETERODYNE SPECTROMETERS

Molecule	Band	Frequency	IRHS Reference
ClO	Fund.	840 cm^{-1}	21, 22
CO_2	$(\nu_3-2\nu_2)_{I,II}$	820-1100	10, 11, 23, 24
OCS	ν_1	859	22
O_3	ν_3	1042	25
N_2O	$\nu_3-\nu_1$	939	
H_2O	Rot.	850-1100	
HO_2	ν_3	1100	
NH_3	ν_2	933,968	18, 26, 27
PH_3	ν_2	992	
H_2CO		~1000	
GeH_4	ν_2	931	
SiH_4	ν_4	914	
HNO_3		~850	22
H_2SO_4		~960	
C_2H_4	ν_7	~949	28
C_2H_3	ν_9	820	29

and others

Figure Captions

Fig. 1. Planetary radiance is plotted as a function of wavenumber. The thermal emission from terrestrial planets is seen to peak near 1000 cm^{-1}.

Fig. 2. Basic principles of infrared heterodyne detection. See text for details.

Fig. 3. The Goddard Space Flignt Center infrared heterodyne spectrometer optical front end.

Fig. 4. The Goddard 128-channel RF spectral line receiver.

Fig. 5. Measurements on Venus at three different resolving powers: a) Photometric measurements ($\lambda/\Delta\lambda \sim 1$) yield a broadband radiance plot. b) FTS measurements near 1000 cm^{-1} ($\lambda/\Delta\lambda \sim 4000$) resolve individual CO_2 absorption lines. c) Infrared heterodyne spectrometer measurements on a single CO_2 line with $\lambda/\Delta\lambda \sim 10^6$ and 10^7 reveal a strong CO_2 core emission.

Fig. 6. The spectral range covered with CO_2 isotope gas laser transitions taken from Ref. 16.

Fig. 7. Spectral intensity of blackbody sources and the signal-to-noise ratio possible with an infrared heterodyne spectrometer ($\Delta = 7$, $B = 25$ MHz, $\tau =$ 1 hr.)

Fig. 8. Formation of atmospheric lines and the radiative transfer equation.

Fig. 9. Infrared heterodyne measurements of CO_2 spectral features on Mars. The measured broad absorption line (Fig. 9A) is composed of transmitted surface intensity and atmospheric self-emission. The core emission measured at 5 MHz resolution, (Fig. 9B) is composed of high altitude non-thermal emission and naturally occuring CO_2 laser emission. From the linewidth a local kinetic temperature of 128K is retrieved.

Fig. 10. Infrared heterodyne map of the R8 CO_2 line on Mars. The observing

geometry on the planet is given at the upper right. The planetary disk was ~13 arc-sec while the heterodyne field of view (full width at half maximum) was ~1.8 arc-sec.

Fig. 11. The geometry for observations of Jovian stratospheric ethane. The ~2 arc-sec field of view was centered on the central meridian and 70^{o} south latitude.

Fig. 12. Jovian ethane lines measured at 25 MHz resolution (circles). The solid curve represents the best fit to the data using the model atmosphere in Fig. 13 and an appropriate planetary rotational broadening function.

Fig. 13. The Jupiter south pole atmospheric model used in the retrieval of the C_2H_6:H_2 mixing ratio from heterodyne measurements near 12μm.

Fig. 14. Earth's atmospheric transmission near 855 cm^{-1} as measured by Goldman et al.[41] The spectral regions about P12 and P8 $^{14}C^{16}O_2$ laser transitions show a transmittance close to 1 and thus were found to be excellent regions for infrared heterodyne measurements of atmospheric CℓO.

Fig. 15. (a) left. Observed and modelled spectra of the terrestrial atmosphere near the P12 $^{14}CO_2$ laser line. The frequency resolution is 25 MHz and the spectra are displayed as transmittance vs. the frequency difference from 856.515 cm^{-1}. The modelled spectrum based on the accepted atmospheric temperature profile, molecular abundances and molecular parameters is displaced downward for clarity, and the expected line of $^{35}C\ell O$ is indicated. (b) right. Observed and modelled spectrum, centered on the R9.5 CℓO line. The frequency resolution in the observed spectrum is 5 MHz and the modelled spectrum is displayed with infinite resolution. The residual differences between the observations and the modelled spectrum without CℓO are shown, and are compared with the expected CℓO line.

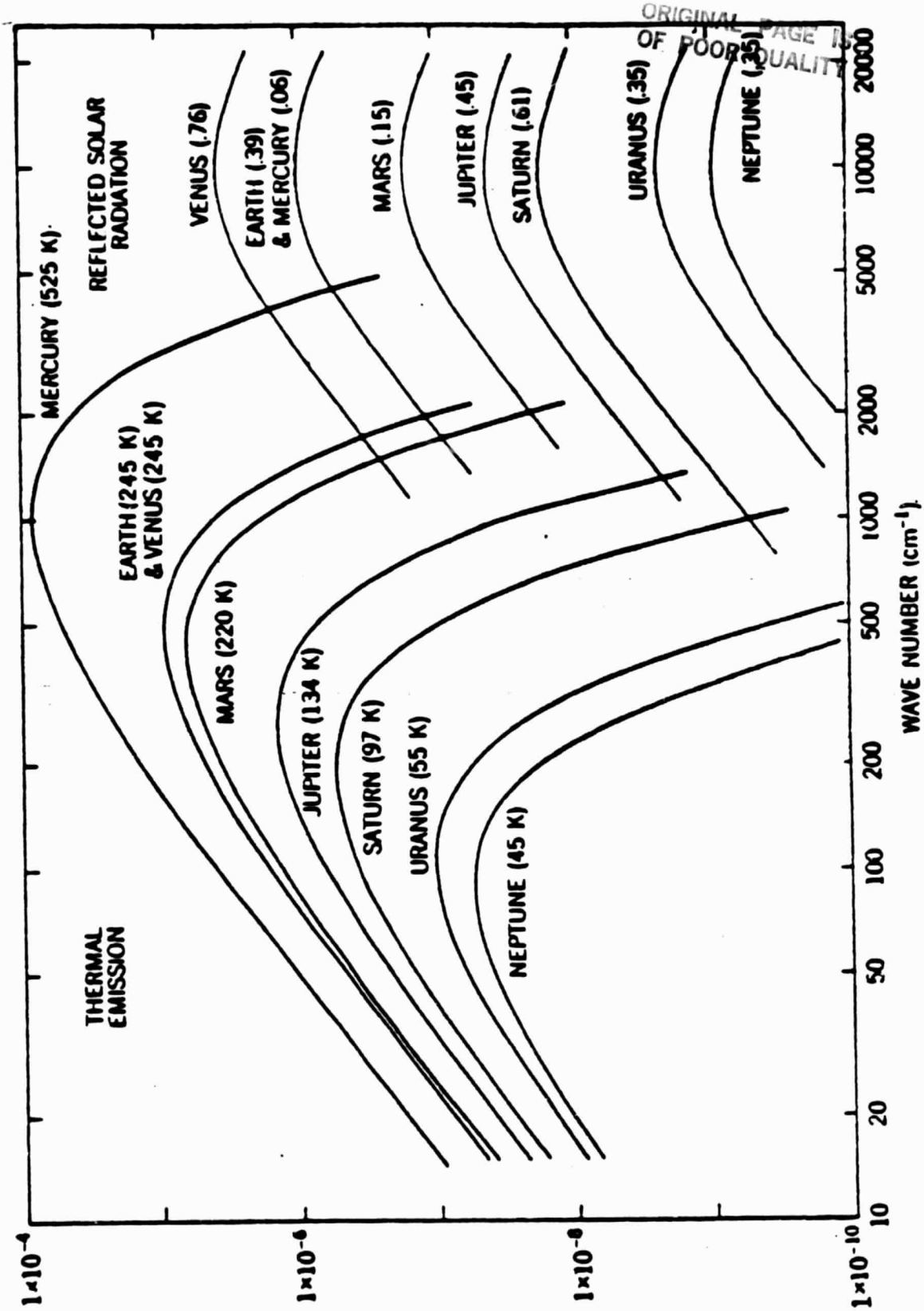

Figure 1

INFRARED HETERODYNE DETECTION

$$E = E_{LO}\, e^{i\omega_{LO}t} + E_S\, e^{i\omega_S t}$$

$$R_{IR} \propto |E|^2 = E_{LO}^* E_{LO} + E_S^* E_S + 2\, E_{LO} E_S \cos(\omega_{LO} - \omega_S)t$$

$$S_{HET} \propto P_{LO} P_S \langle \cos^2 \omega_{IF}\, t \rangle$$

$$N_{SNL} \propto B P_{LO}$$

SIGNAL TO NOISE IN SHOT NOISE LIMIT:

$$S/N = \frac{P_S}{h\nu B} \quad \text{at the IF}$$

AFTER INTEGRATION FOR TIME τ :

$$S/N = \frac{P_S}{\Delta h\nu} \left(\frac{\tau}{B}\right)^{1/2}$$

Δ = SYSTEM DEGRADATION FACTOR

$$NEP = \frac{\Delta h\nu}{\sqrt{B\tau}} \quad \frac{\text{Watts}}{\text{Hz}}$$

$$NEF = \frac{\Delta}{\sqrt{B\tau}} \quad \frac{\text{Photons}}{\text{Sec Hz}}$$

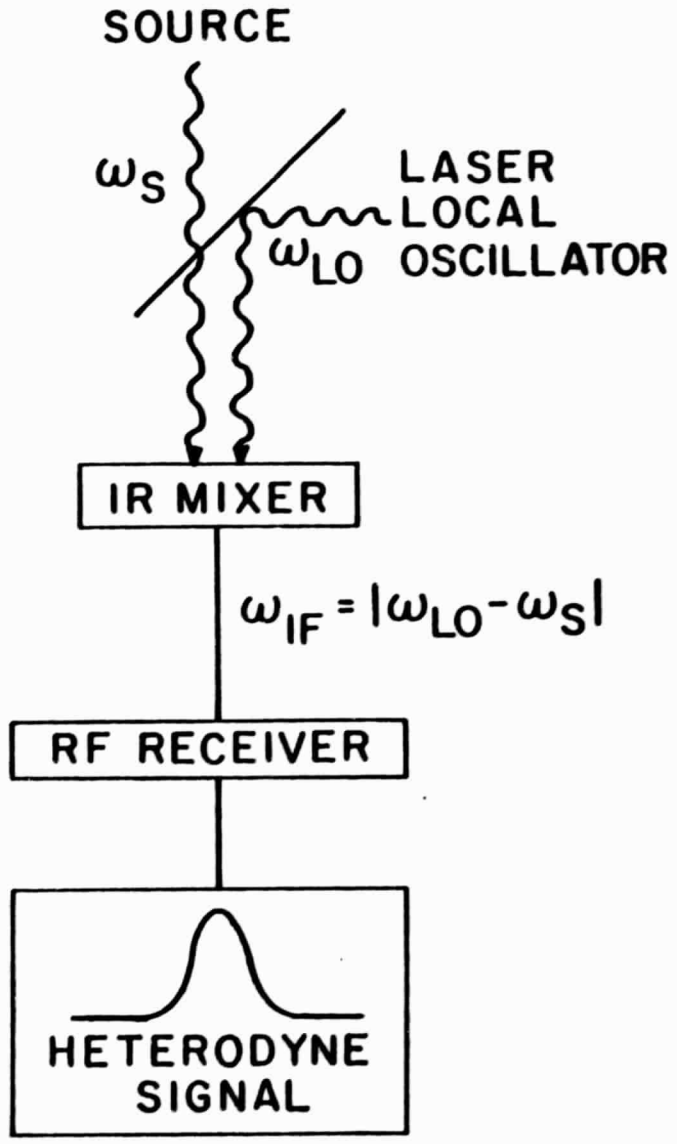

Figure 2

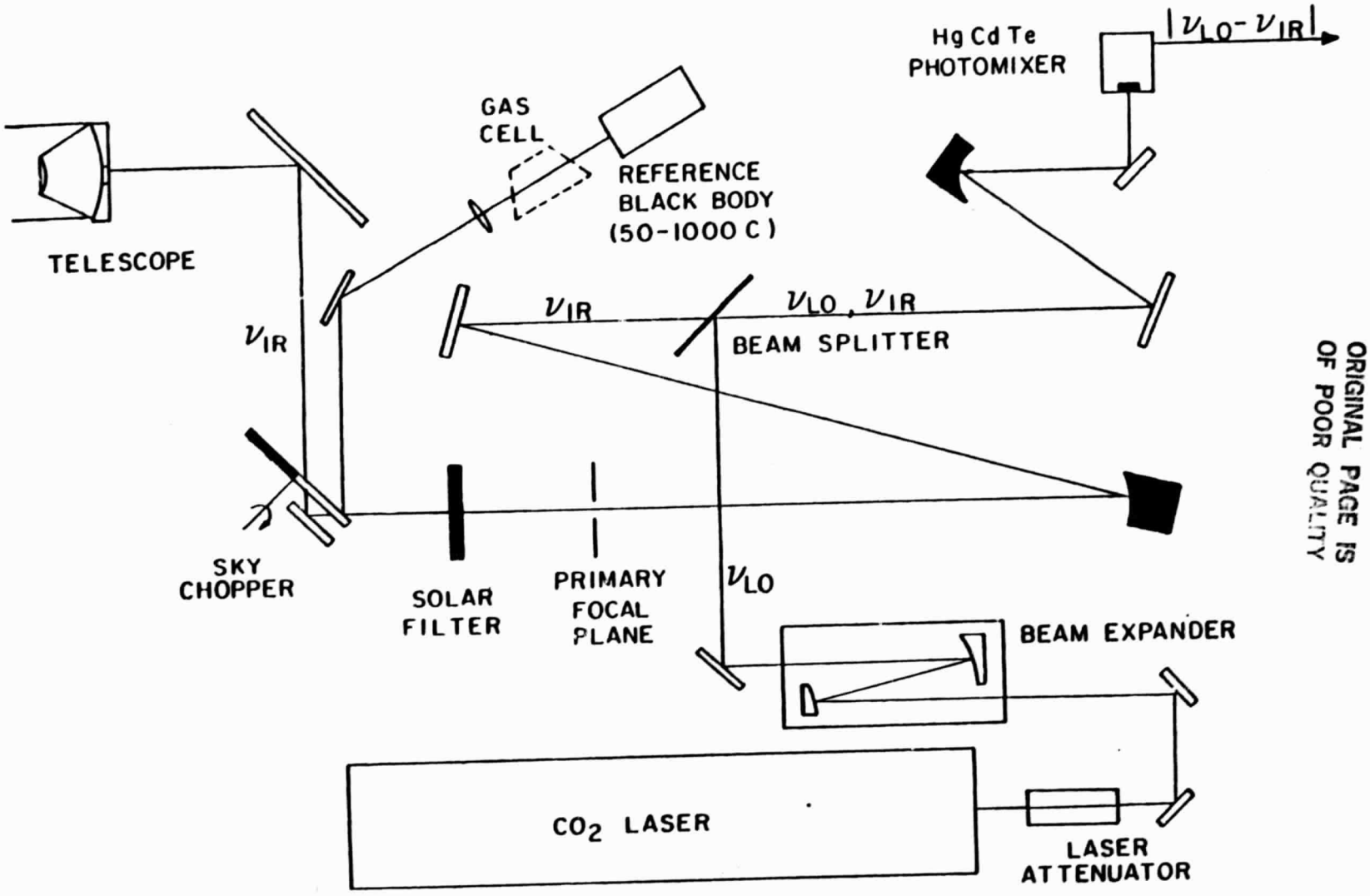

Figure 3

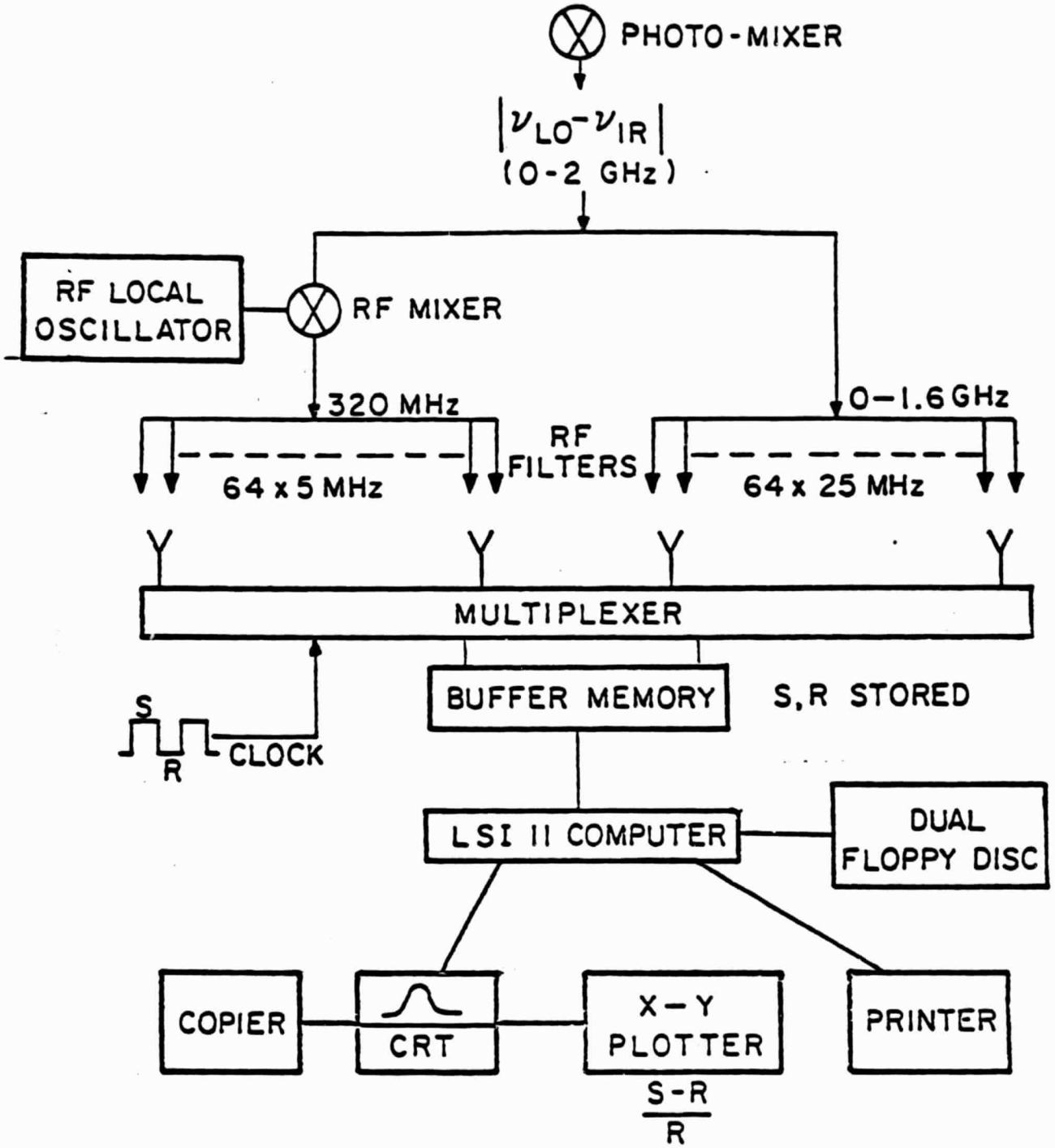

Figure 4

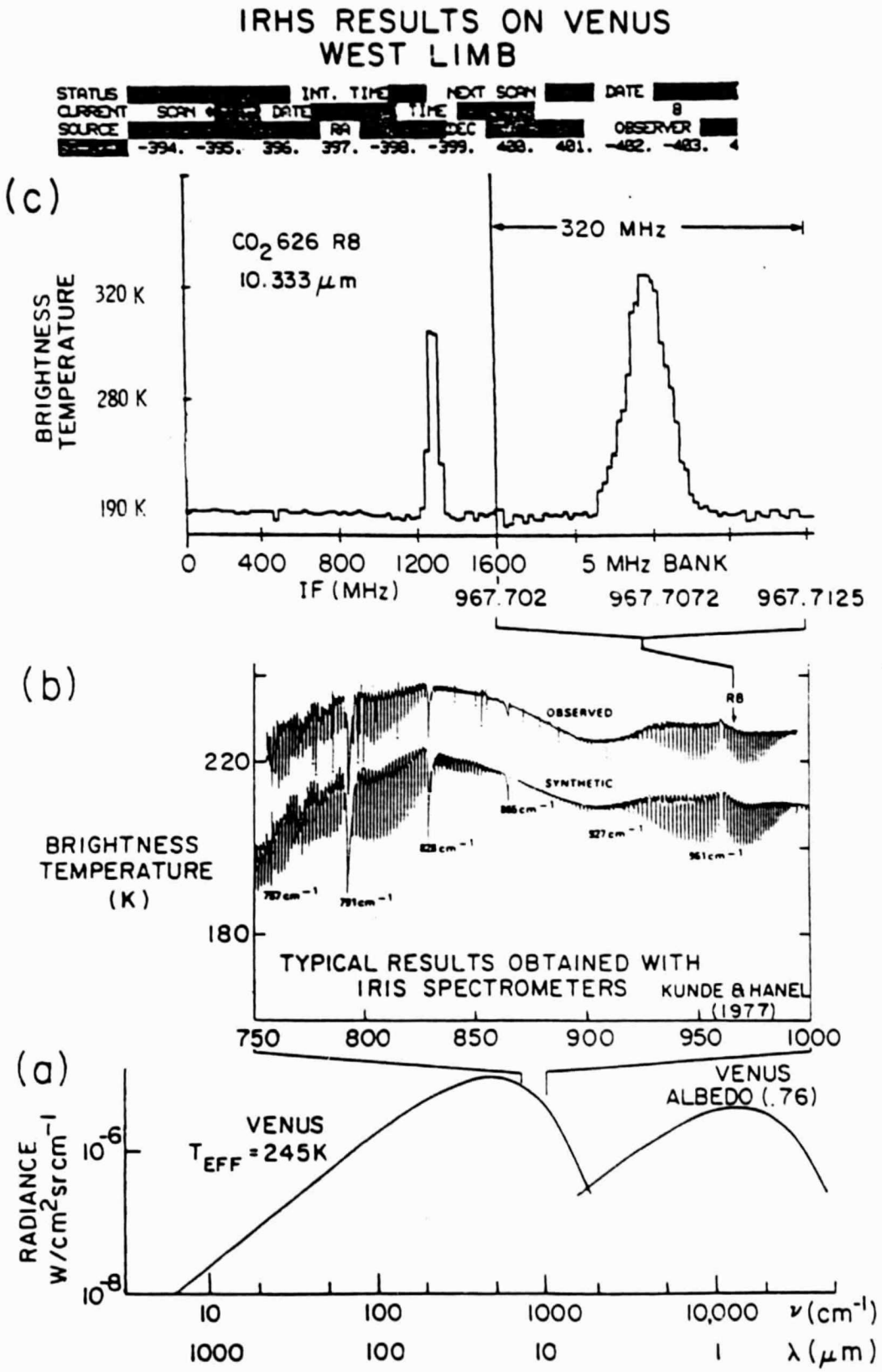

Figure 5

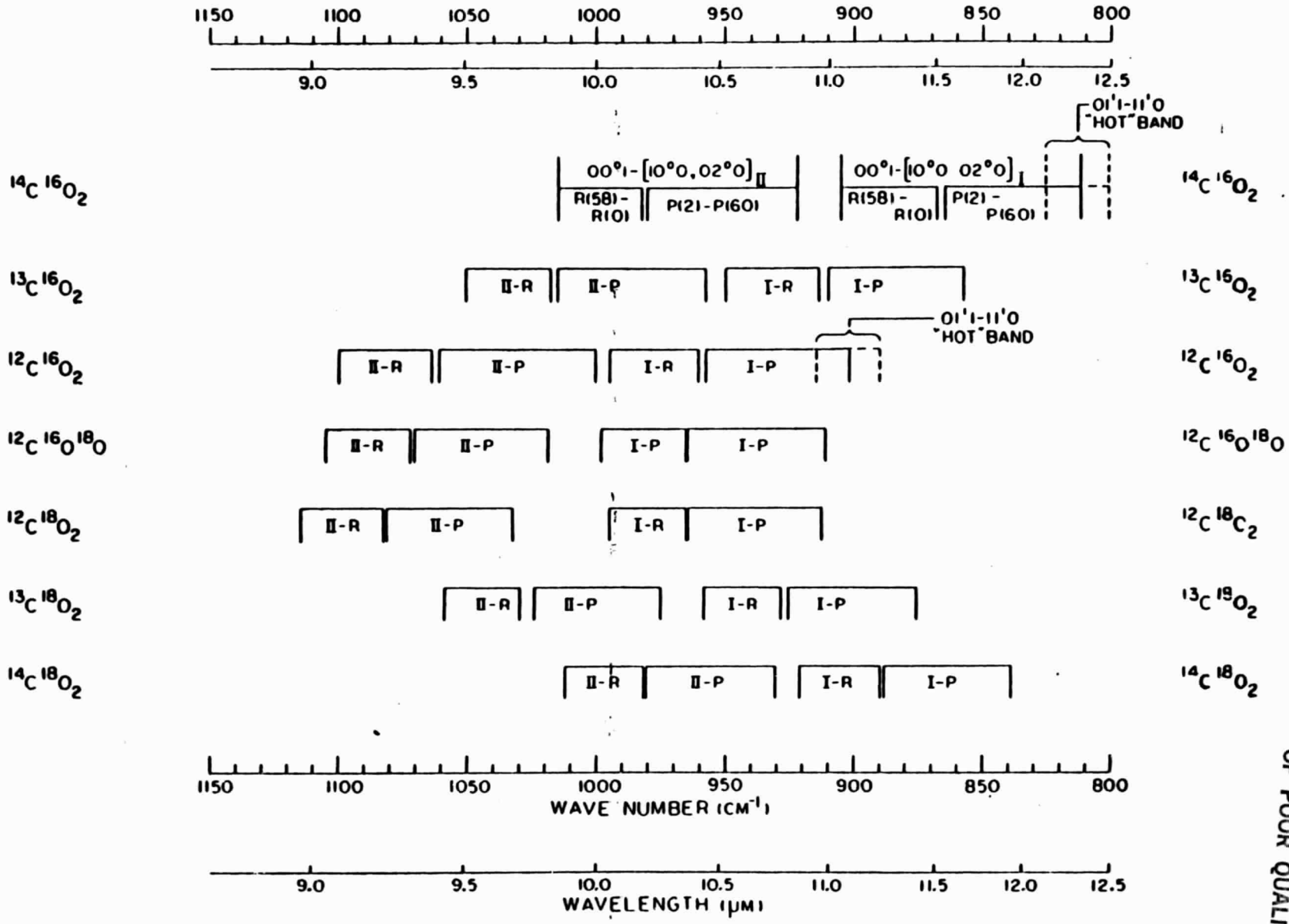

CO_2 ISOTOPE LASER TRANSITIONS

17

FREED, BRADLEY, AND O'DONNELL (1980)

Figure 6

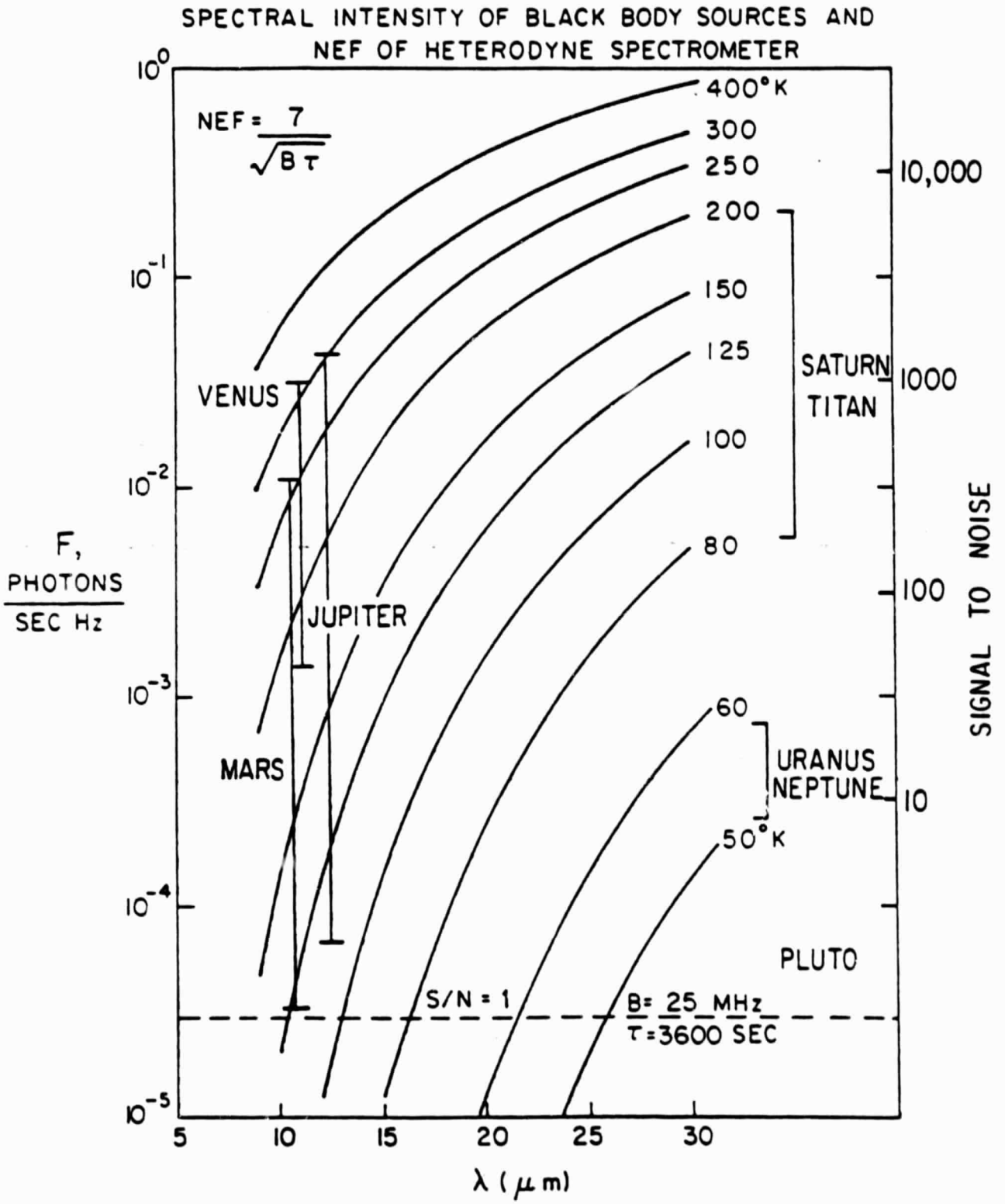

Figure 7

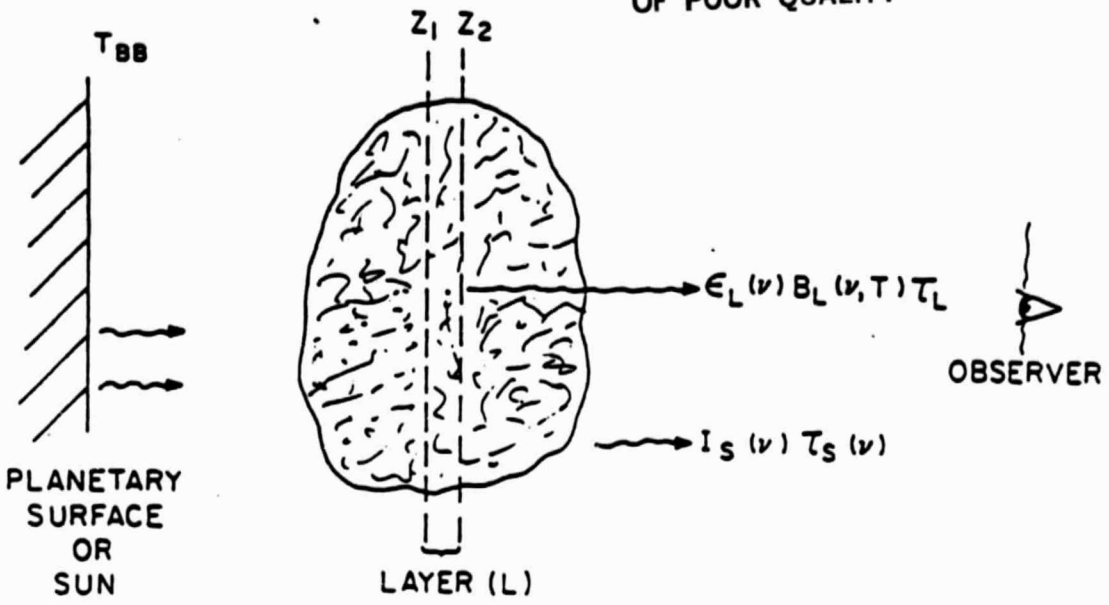

INTERVENING ATMOSPHERE

RADIATIVE TRANSFER EQUATION:

$$I_{TOTAL}(\nu) = I_s(\nu, T_{BB})\, \tau_s(\nu) + \int_{\tau_s}^{1} B(\nu, T)\, d\tau\,(P, T)$$

TRANSMITTED SURFACE INTENSITY

ATMOSPHERIC SELF-EMISSION

INVERSE OR ITERATIVE SOLUTION YIELDS:

T(z) if n(z) is known

n(z) if T(z) is known

IF S, ν_o, α_L, α_D, are known!

Figure 8

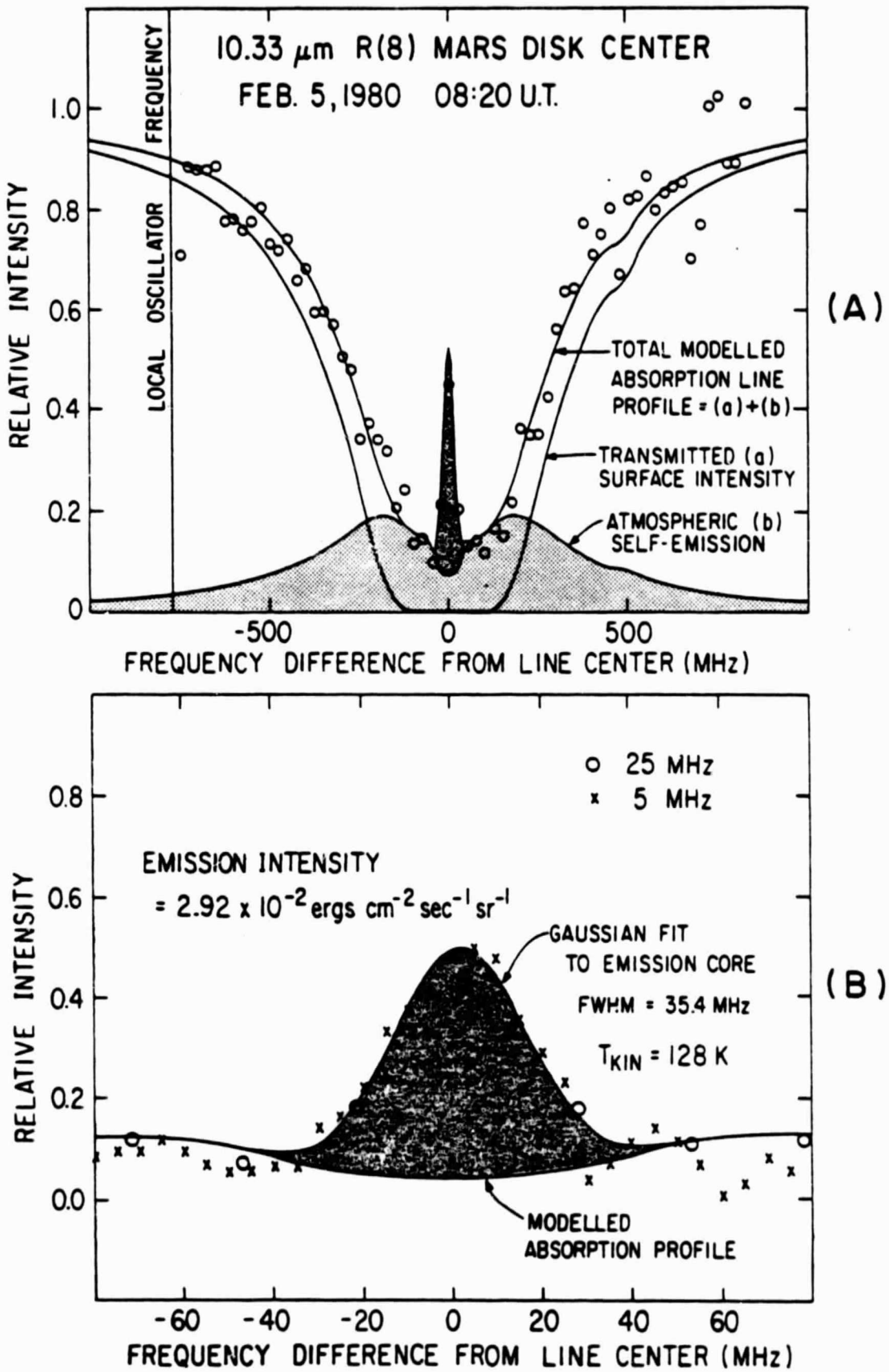

Figure 9

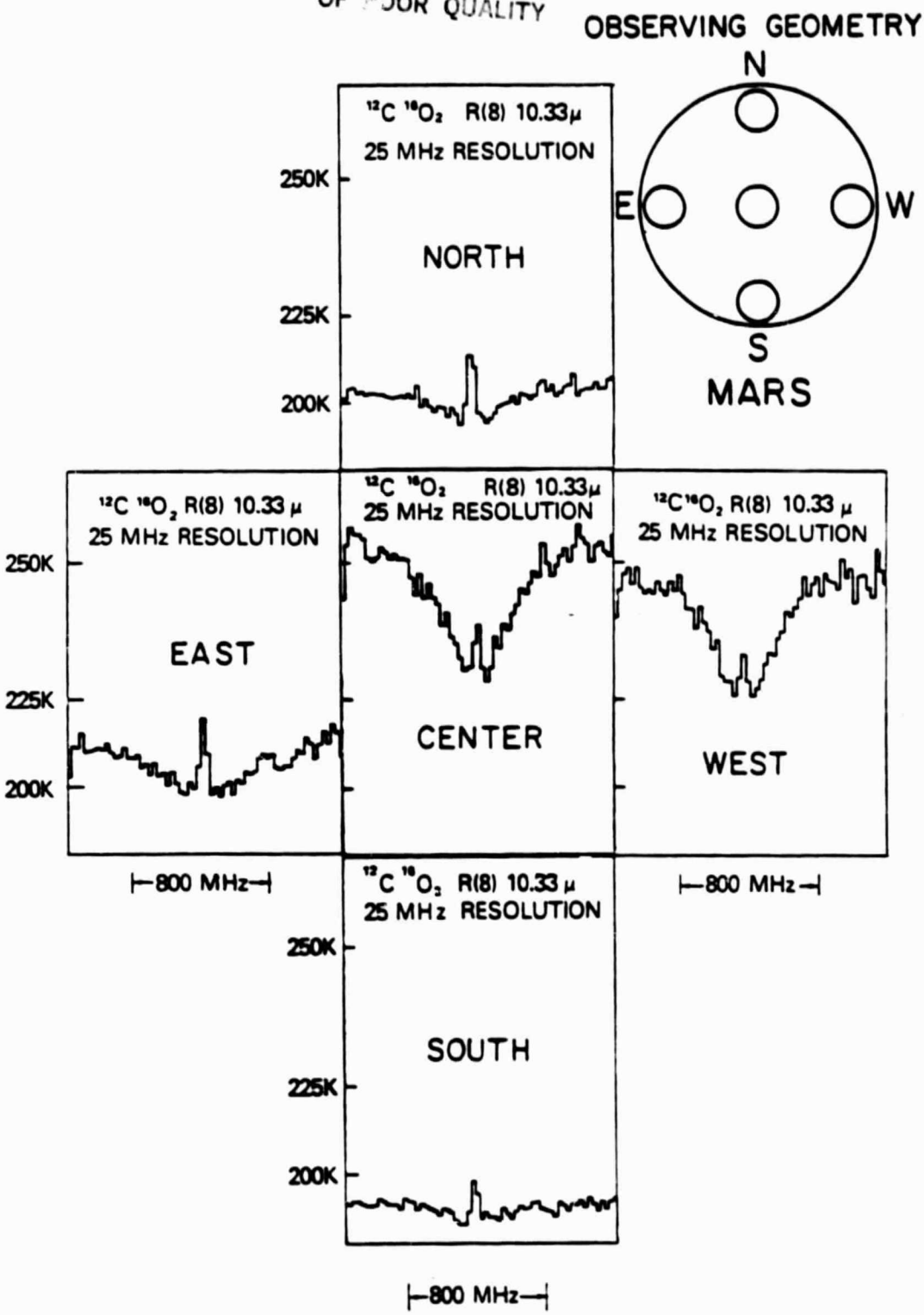

CO_2 LINE PROFILE MAP
OF MARS
FEB, 1980

Figure 10

GEOMETRY FOR JOVIAN ETHANE OBSERVATIONS

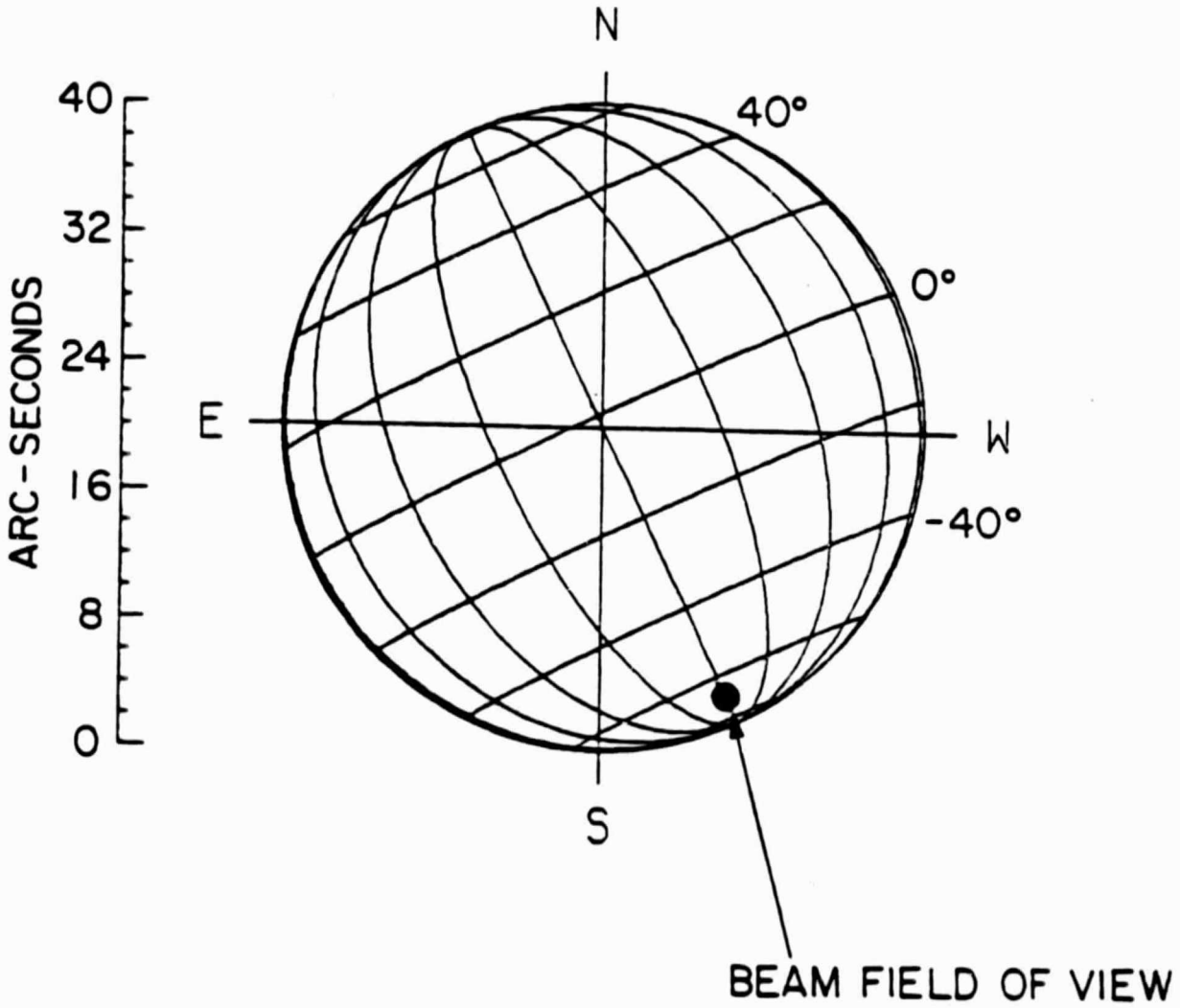

JUPITER 22 MAY 1981 4:49 UT

Figure 11

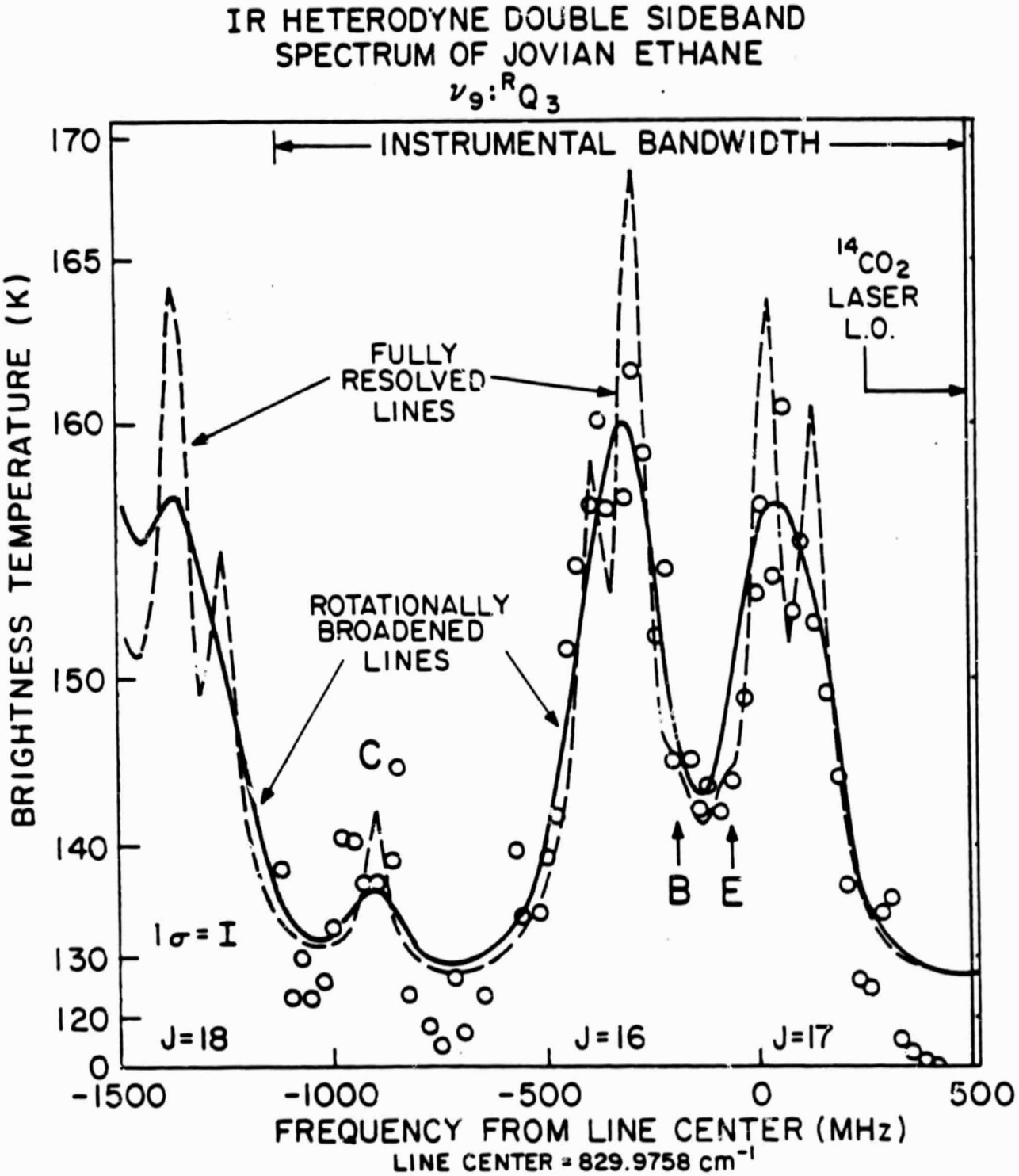

Figure 12

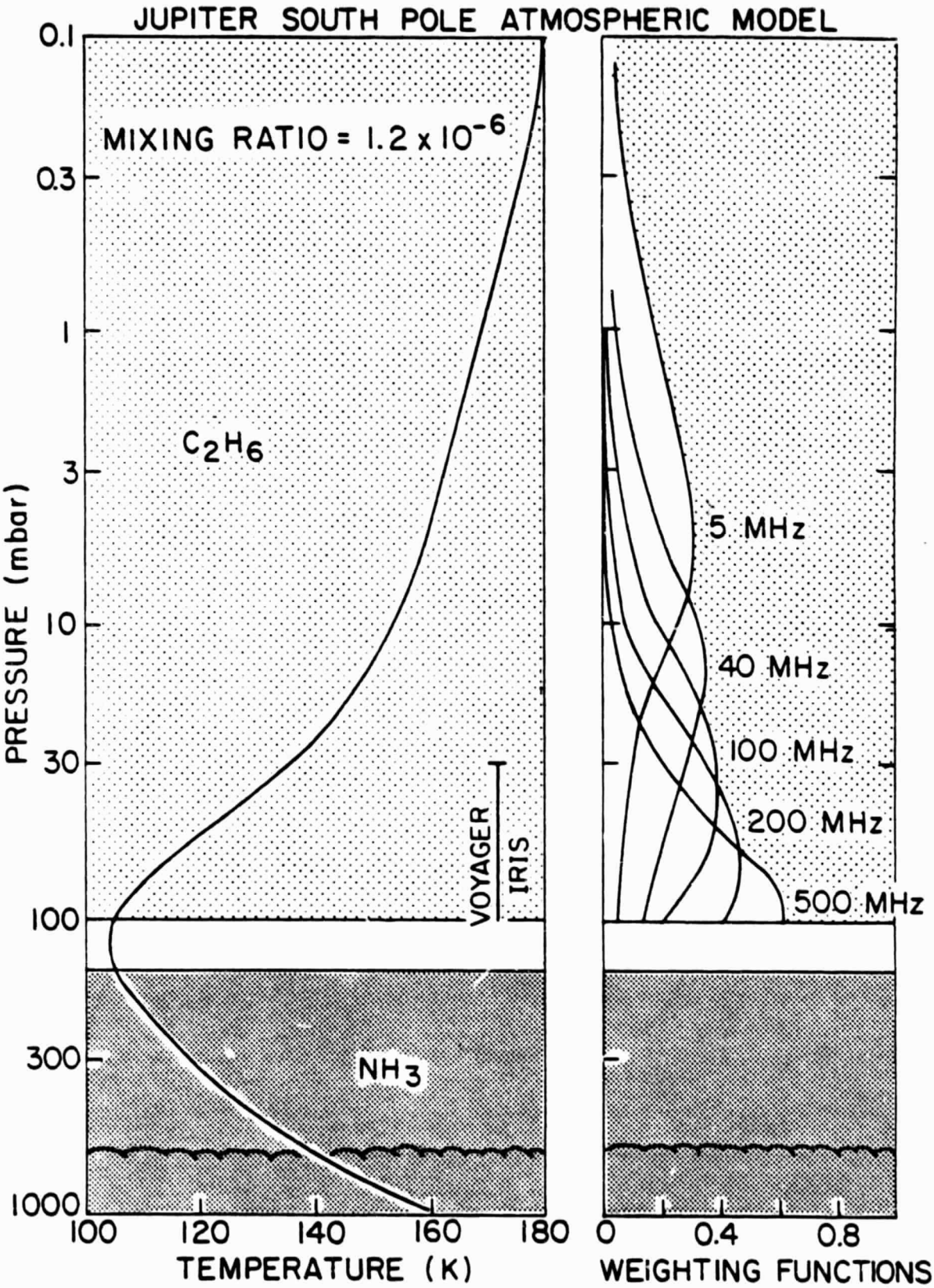

Figure 13

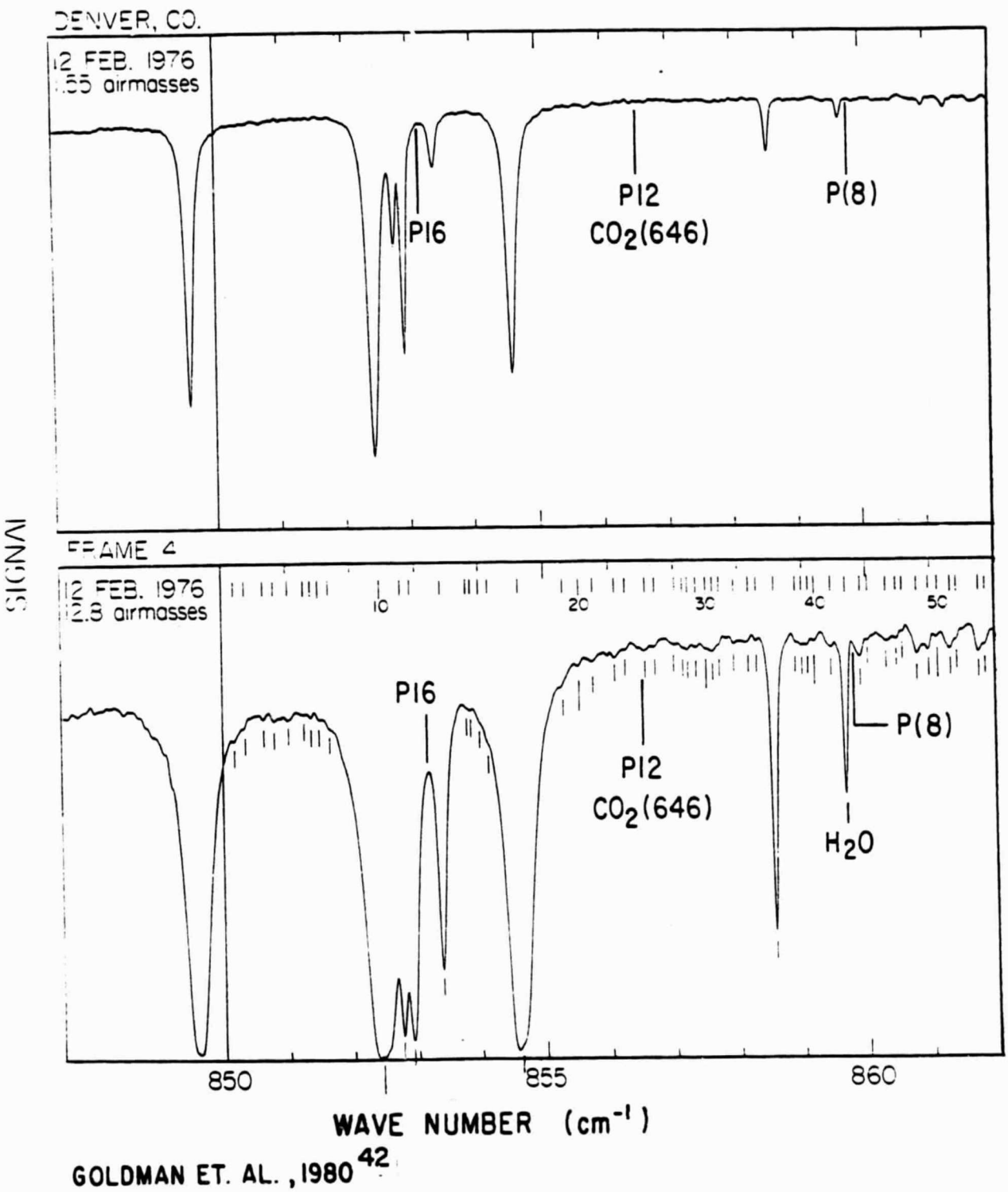

GOLDMAN ET. AL., 1980[42]

Figure 14

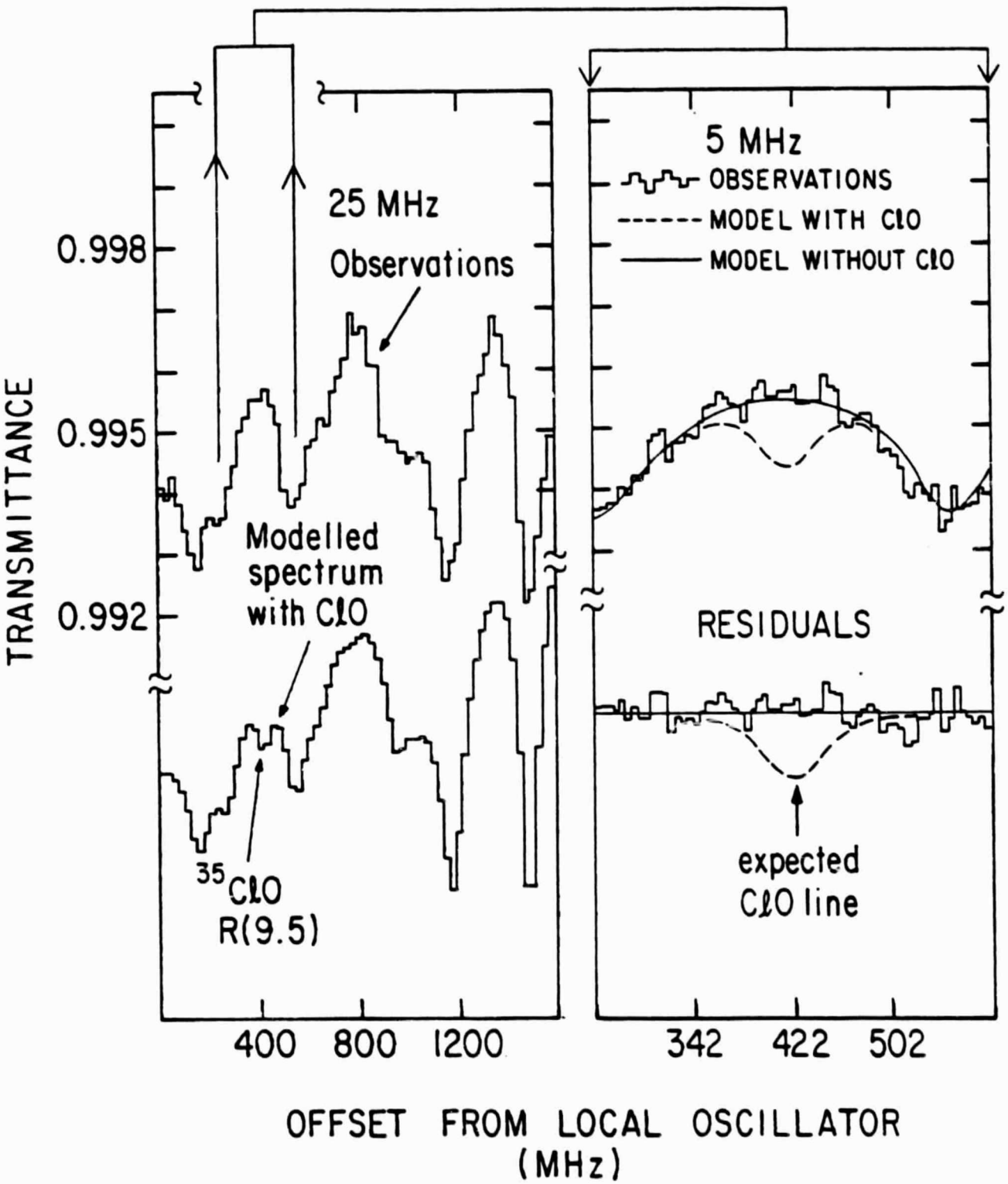

Figure 15